Available online at www.sciencedirect.com
SCIENCE DIRECT®
International Journal of Heat and Fluid Flow 26 (2006) 80–94
International Journal of HEAT AND FLUID FLOW
www.elsevier.com/locate/ijhff

Three-dimensional numerical study of flow and heat transfer from a cube placed in a uniform flow

A.K. Saha *

Department of Mechanical Engineering, Louisiana State University, Baton Rouge, LA 70803, USA

Received 5 July 2004; accepted 16 May 2005
Available online 11 July 2005

Abstract

The fluid flow and heat transfer from a stationary cube placed in a uniform flow is studied numerically. The three-dimensional unsteady Navier Stokes and energy equations are solved using higher order temporal and spatial discretizations. Computations are carried out for a Reynolds number range of 50–400. At $Re = 218$, the symmetry seen at $Re = 216$ breaks down in one of the orthogonal planes while remains symmetric on the other thus showing a planar symmetry. The flow experiences a Hopf bifurcation at a Reynolds number between 265 and 270 and becomes unsteady. The thermal field also shows all the transitions same as those of flow transitions. The drag coefficient decreases while the heat transfer shows an increasing trend with Reynolds number. The transition from a steady to an unsteady flow does not show any significant increase in the heat transfer. Both the flow and thermal fields show multiple frequencies at high Reynolds number and the number of frequencies increases with the increase in Reynolds number. The instantaneous flow and temperature field are seen to deviate from planar symmetry at $Re = 400$.

Keywords: Cube; Wakes; Transition; Vortex shedding

1. Introduction

The complex transition phenomenon of the wake of a three-dimensional bluff object has become an important topic of research. Literature on flow past a three-dimensional body indicates that vortex shedding due to a sphere differs from that of a two-dimensional bluff body namely, circular cylinder. Similarly, the flow past a cube, which is a three-dimensional bluff body, shows significant variation in its shedding mechanism and transition sequence compared to its two-dimensional counterpart, the square cylinder (Saha, 2004).

The sphere wake remains steady and symmetric up to $Re \sim 210$ (Natarajan and Acrivos, 1993; Johnson and Patel, 1999; Magarvey and Bishop, 1961; Nakamura, 1976) beyond which the symmetry breaks and the wake becomes asymmetric (asymmetric on one plane and symmetric on the other) but remains steady. With increasing Reynolds number, the steady non-axisymmetric flow experiences an additional transition, a temporal one called Hopf bifurcation. Most of the studies reported this temporal transition Reynolds number to be in the range of $270 < Re < 400$ (Thomson et al., 2001; Tomboulides and Orszag, 2000; Johnson and Patel, 1999). The measured dominant non-dimensional frequency, called Strouhal number (St), shows a strong periodic wake up to a Reynolds number of 420 and has been found to be in the range of $0.15 < St < 0.17$ (Kim and Durbin, 1988).

At a relatively higher Reynolds number, the symmetry on one plane and asymmetry on the other breaks down to a total asymmetric flow past a sphere. The loss of planar symmetry of the wake at higher Reynolds

* Present Address: Department of Mechanical Engineering, Indian Institute of Technology Kanpur, Kanpur, UP 208 016, India. Tel.: +91 512 259 7686; fax: +91 512 259 0007.
E-mail address: aksaha@iitk.ac.in

0142-727X/$ - see front matter © 2005 Elsevier Inc. All rights reserved.
doi:10.1016/j.ijheatfluidflow.2005.05.002

Nomenclature

Ar	face area of the cube
B	cube dimension
C_D	drag coefficient, $\mathscr{D}/(\frac{1}{2}\rho u_\infty^2 \mathrm{Ar})$
C_S	side force coefficient, $\mathscr{L}/(\frac{1}{2}\rho u_\infty^2 \mathrm{Ar})$
$\mathscr{D}$	drag force on the cube, $\sum_1 \tilde{P}\delta y\delta z - \sum_2 \tilde{P}\delta y\delta z$
f	frequency of vortex shedding
h	heat transfer coefficient
H	lateral dimension of the flow domain
K	thermal conductivity
$\mathscr{L}$	side force on the cube, $\sum_{s1}\tilde{P}\delta x\delta y - \sum_{s2}\tilde{P}\delta x\delta z$ or $\sum_{s3}\tilde{P}\delta x\delta y - \sum_{s4}\delta x\delta y$
Nu	Nusselt number, $hB/K = \partial\theta/\partial n$
p	static pressure
$\tilde{P}$	pressure distribution on the surface of the cube
Pr	Prandtl number, ν/α
Re	Reynolds number, $\rho u_\infty B/\mu$
St	Strouhal number, fB/u_∞
T	time period of oscillation, $1/f$
t	time
u, v, w	streamwise, transverse and spanwise components of velocity
x, y, z	streamwise, transverse and spanwise coordinates
u_c	convective velocity at the outlet

Greeks

α	thermal diffusivity
μ	dynamic viscosity
ν	kinematic viscosity
ρ	density
ω_i	instantaneous vorticity vector, $\varepsilon_{i,j,k}\frac{\partial u_k}{\partial x_j}$
θ	non-dimensional temperature, $(T - T_\infty)/(T_w - T_\infty)$

Subscripts

∞	freestream
w	wall
1, 2	forward and rear sides of the cube
s1, s2, s3, s4	four transverse sides of the cube

number has been shown by Mittal (1999). The phase relationships between the two side forces is used to analyse the loss of planar symmetry. His results reveal that the wake loses its planar symmetry once the Reynolds number crosses a value in the range of 350–375 which is lower than the reported value of $Re \sim 420$ by Sakamoto and Haniu (1990) and $Re \sim 500$ by Tomboulides and Orszag (2000).

Recent numerical and experimental study by Johnson and Patel (1999) has revealed many interesting transition phenomenon of the sphere wake. They considered a wide range of Reynolds number and presented the behaviour of wake with increasing Reynolds number. Their results also reveal similar findings viz. different transition scenario and the corresponding Reynolds numbers as presented by other researchers (Magarvey and Bishop, 1961; Mittal, 1999; Nakamura, 1976).

All of the studies referred above reported only the flow field data. There is also a few studies that provide both the flow, heat and mass transfer around spherical shaped body such as drops and particles but most of them are limited to low Reynolds number ($\leqslant$100) flow simulations (Sayegh and Gauvin, 1999; Renksizbulut and Yuen, 1983). The heat transfer results of Sayegh and Gauvin (1999) compare well with the experimental data of Ranz and Marshall (1952) and Whitaker (1972). Recently, Bagchi et al. (2001) has carried out a DNS (Direct Numerical Simulation) study of the flow and heat transfer past a sphere for Reynolds numbers up to 500. The different transitions in sphere wake are well captured in their simulations. They have done both two-dimensional axisymmetric and three-dimensional simulations and shown that local Nusselt number distribution on the sphere surface shows a big difference while the difference in surface-averaged Nusselt number between the two simulations was small.

The study of heat transfer and flow past a two-dimensional bluff body namely square cylinder has been the subject of extensive research because of its increased engineering importance. There is a large volume of literature available on fluid flow study on this particular geometry. Unlike the sphere and cube wakes, the square cylinder wake with a uniform approach flow does not undergo spatial transition in the steady regime. The spatial transition in the form of different modes of shedding occurs after the flow becomes unsteady (Saha et al., 2003). Kelkar and Patankar (1992) have carried out linear stability analysis of flow and heat transfer past a square cylinder up to a Reynolds number of 100 and found a critical Reynolds number at which the flow becomes unsteady to be 53. Recently, the heat transfer and fluid flow for a square cylinder has been investigated by Sharma and Eswaran (2004). Their study reports the correlation of Nusselt number and Reynolds number and detailed analysis of the two-dimensional steady and unsteady flow ($1 \leqslant Re \leqslant 160$).

Most of the above studies on both sphere and square cylinder is limited to laminar flow. Though the scope of the present study is for laminar flow, some discussion on turbulent flow past various bluff bodies will shed more light on the separation mechanism and the related heat transfer of various bluff bodies at high Reynolds

number. The behaviour of sphere wake at high Reynolds number is seen to be almost identical to circular cylinder wake. At Reynolds number above 800, the wake exhibits multiple frequencies because of its transition to turbulence (Sakamoto and Haniu, 1990; Achenbach, 1974). Similar to circular cylinder wake, at Reynolds number of about 3.7×10^5, the boundary layer on the sphere surface becomes turbulent and delays its separation reducing the drag coefficient (this phenomenon is also called drag crisis) significantly (Maxworthy, 1969). Similar observation is also reported numerically by Constantinescu and Squires (2004). The study of turbulent heat transfer past a sphere is limited. One of such studies is by Whitaker (1972). Though the investigation of cylinder and sphere wakes are done at high Reynolds number, the detail study of the turbulent wake past a square cylinder has only been done up to a Reynolds number of 24,000 and is well documented in Lyn et al. (1995). Unlike flow past circular cylinder or sphere, the boundary layer formed at the front face of the square cylinder does not encounter any separation delay as it has definite lines of separation at its leading/front face edges. However, separation at the trailing face edges is possible after reattachment on the side faces of the cylinder. A very few studies on turbulent heat transfer past a square cylinder is available and one such investigation is carried out by Igarashi (1985) for a Reynolds number range of 5.6×10^3–5.6×10^4. He has done a detail experimental study of heat transfer from the cylinder along with flow visualization to support his claims on heat transfer.

The difference in separation mechanism and the related integral parameters like Strouhal number, side and drag forces is expected because of the fixed lines of separation for cube flow while for a sphere wake, they vary along the sphere surface depending on the Reynolds number and the other flow conditions such as turbulence and uniformity of the approach flow, sphere surface roughness etc. There is a few studies available on flow past a stationary cube. Raul et al. (1990) have carried out both numerical and experimental study for flow past a stationary cube at Reynolds number (based on cube dimension and freestream velocity) range of 10–100. They found a good agreement for the drag coefficient between the cube drop experiments and the numerical data. In a subsequent study, Raul and Bernard (1991) studied the turbulent flow past a stationary cube for $Re = 2000$ and 14,000 using turbulence model. Their results such as drag, axial velocity and separation points reveal good match with experimental observations of similar bluff body (square cylinder and circular cylinder) flows. Saha (2004) has carried out a detail study of transition sequence for a Reynolds number range of 50–300. The critical Reynolds number corresponding to the different transitions are reported in Saha (2004). The integral parameters like drag coefficient, side force coefficient and the Strouhal number for unsteady flow has been presented in the study. The flow topology and their relation to the transitions are also discussed. Only flow field data is provided in the calculation and no heat transfer calculation was undertaken in Saha (2004).

As it has been discussed in Saha (2004), the cube possesses symmetry about three orthogonal axes. Therefore, the flow past a cube can have symmetry on two orthogonal planes that are orthogonal to the streamwise axis. In the present study, orthogonal-symmetric or simply symmetric flow corresponds to the symmetry of flow about the streamwise centreline on these two orthogonal planes. On the other hand, asymmetric flow refers to the loss of discrete rotational symmetry in the sense that the flow is symmetric about the streamwise centreline on one orthogonal plane while it becomes asymmetric on the other orthogonal plane.

The present study is aimed at the three-dimensional numerical computations of the flow and heat transfer past a stationary cube placed in an infinite medium for Reynolds number (based on inlet velocity and the cube dimension) range of 50–400. A DNS study is undertaken to see the effect of the different transitions on heat transfer and to investigate the flow structure and heat transfer characteristics at high Reynolds number. The results are discussed in contrast with that of sphere and square cylinder wakes. The time-averaged integral parameters such as side force and drag coefficients, Strouhal number and Nusselt number are computed and compared to that of sphere and square cylinder.

2. Mathematical model and numerical technique

The unsteady three-dimensional Navier–Stokes equations along with the incompressibility constraint and energy equations have been numerically solved in the present study. The equations for continuity, momentum and energy in dimensionless form may be expressed as:

$$\frac{\partial u_i}{\partial x_i} = 0 \tag{1}$$

$$\frac{\partial u_i}{\partial t} + \frac{\partial (u_j u_i)}{\partial x_j} = -\frac{\partial p}{\partial x_i} + \frac{1}{Re}\frac{\partial^2 u_i}{\partial x_j^2} \tag{2}$$

$$\frac{\partial \theta}{\partial t} + \frac{\partial (u_j \theta)}{\partial x_j} = \frac{1}{Re\,Pr}\frac{\partial^2 \theta}{\partial x_j^2} \tag{3}$$

In the above equations the velocities are non-dimensionalized with the average velocity at inlet u_∞, all lengths with the obstacle height B, time with u_∞/B, pressure by ρu_∞^2 and temperature by $(T - T_\infty)/(T_w - T_\infty)$, where T_∞ and T_w are the freestream and wall temperature respectively. The working fluid chosen in the present study is air whose Prandtl number is 0.7.

The geometry and the relevant dimensions considered for analysis are schematically shown in Fig. 1. The

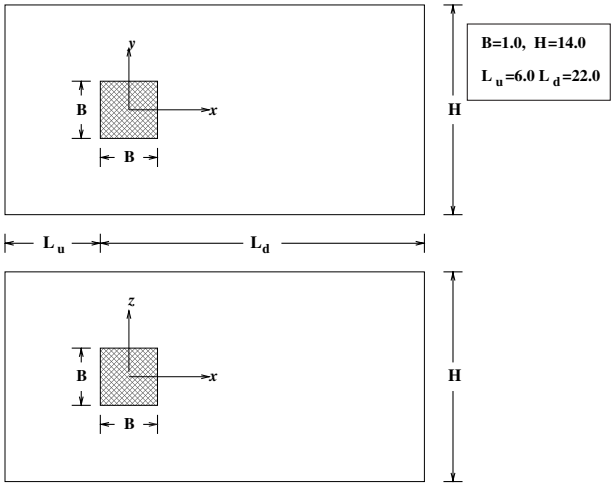

Fig. 1. Three-dimensional computational model.

dimensions related to the geometry in the figure are $B = 1.0$, $L_u = 6.0$, $L_d = 22.0$ and $H = 14.0$. In relation to this figure, the boundary conditions employed for the present investigation are: (i) the confining surfaces are modeled as the free-slip, for example, at the transverse confining surfaces, $y = \pm H/2$, $\partial u/\partial y = v = \partial w/\partial y = 0$, (ii) at the inlet, a constant streamwise velocity has been used with other components of velocity being set to zero (iii) At the outlet, the following convective outflow boundary conditions have been employed (Orlanski, 1976):

$$\frac{\partial u}{\partial t} + u_c \frac{\partial u_i}{\partial x} = 0 \tag{4}$$

where u_c, the convective velocity is the celerity of vortices leaving the outflow plane. The value of u_c can be taken as either the absolute local velocity at the outflow plane or a fixed positive velocity with which the vortices are being convected out of the domain. For the present study a value of 0.8 for u_c has been used. For all the solid surfaces of the cube, the no-slip boundary condition ($u = v = w = 0$) has been used. For temperature boundary conditions, cube walls are kept at constant wall temperature of $\theta = 1.0$. At inlet, $\theta = 0.0$, corresponding to freestream temperature, is prescribed. The confining surfaces are modeled as adiabatic surfaces, ($y = \pm H/2$, $\partial\theta/\partial y = 0$). At the outlet, convective boundary condition similar to Eq. (4) has been used.

The differential equations (1) and (2) have been solved on a staggered grid by the MAC (Marker and Cell) algorithm of Hoffman and Benocci (1994). Once the momentum equations are solved, the temperature field is obtained by solving the energy equation (Eq. (3)). In the present study, advection and diffusion terms have both been approximated by the second order central differencing scheme while the second order Adam–Bashforth scheme is used for the temporal discretization. The details of the computational methodology have been presented by the author elsewhere (Saha et al., 2000). The grid is clustered near the cube and the spacing is increased in a proper ratio away from the cube surfaces. Most of the computations were carried out using a grid size of $142 \times 78 \times 78$ cells.

The solution is checked for the initial condition dependency. The sensitivity analysis of the domain size has also been carried out using three different domain sizes. The unsteady simulations were also tested for time-step size sensitivity. A typical value of the time-step size of 0.02 is shown to be time-step size independent and is used for most of the simulations. The time-averaged drag coefficient and Strouhal number (for unsteady flow) were the basis for all the analyses. The detail studies of the initial condition, time-step size and domain size dependency have been presented in Saha (2004).

The present code has been validated thoroughly for the flow past a square cylinder by comparing the results with available numerical as well as experimental results at the Reynolds number range of 100–325 (Saha et al., 2003). To get more confidence in the present simulation, the code has also been validated for flow past a cube by comparing with numerical and experimental results available in the literature (Raul et al., 1990) and discussed in full detail in Saha (2004).

The grid independence study has been carried out using three different grid sizes namely, $102 \times 56 \times 56$, $142 \times 78 \times 78$ and $194 \times 104 \times 104$ at a Reynolds number of 300 by comparing the time-averaged values of the lift and drag coefficients, the Strouhal number and Nusselt number. The parameters computed using the three grid sizes along with the number of grid points, N_c, on each side of the cube are listed in Table 1. Strouhal number show equal variation of 2.1% while the total drag coefficient reveals variations of 3.5% and 2.7% for $102 \times 56 \times 56$ and $142 \times 78 \times 78$ respectively with respect to the grid size of $194 \times 104 \times 104$. The corresponding differences in Nusselt number for the two grid sizes are found to be 6.2% and 4.7% respectively. Therefore, the

Table 1
Grid independence test at $Re = 300$

Grid size	N_c	St	$\overline{C}_D$		$\overline{C}_{S,y}$		$\overline{C}_{S,z}$		$\overline{Nu}$
			Form	Friction	Form	Friction	Form	Friction	
$102 \times 56 \times 56$	20	0.095	0.810	−0.035	−0.072	−0.012	0.0	0.0	7.12
$142 \times 78 \times 78$	30	0.095	0.804	−0.023	−0.057	−0.009	0.0	0.0	7.95
$194 \times 104 \times 104$	30	0.097	0.833	−0.030	−0.066	−0.010	0.0	0.0	7.59

grid-size $142 \times 78 \times 78$ is expected to give grid independent results and is used for most of the simulations.

3. Results and discussion

The flow past a sphere undergoes a series of transitions before becoming turbulent. It is expected that the flow past a cube significantly differs from that of a sphere because of the fixed points of separation for a cube. Consequently, the transition sequence and the corresponding critical Reynolds numbers and the flow structures and heat transfer characteristics for a cube are expected to be different from the sphere wake.

3.1. Steady symmetric flow

Long time integration of the governing equations shows that the flow remains steady symmetric up to a Reynolds number of 216. Fig. 2 shows the streamlines, y-component of vorticity and temperature contours all on x–z plane at $Re = 200$. The streamlines plot (Fig. 2(a)) also shows the contours of pressure field (thick solid lines). The flow is seen to separate at the leading edges of the cube with subsequent reattachment before separating fully at the trailing/rear edges of the cube. The symmetric recirculatory region behind the cube is found to grow in size with the increase in Reynolds number (not shown here). Similar to the streamtraces, the pressure field also reveals the symmetric distribution. The bubble size growth causes a decrease in the base suction pressure (BSP) that in turn decreases the drag force. The y-component of vorticity on x–z plane is depicted in Fig. 2(b). The shear layer shows separation from the edges without any roll-up because vorticity components do not show the true vortical structures (Saha, 2004). The isotherms in Fig. 2(c) reveal the distribution of temperature field around the cube. Since the

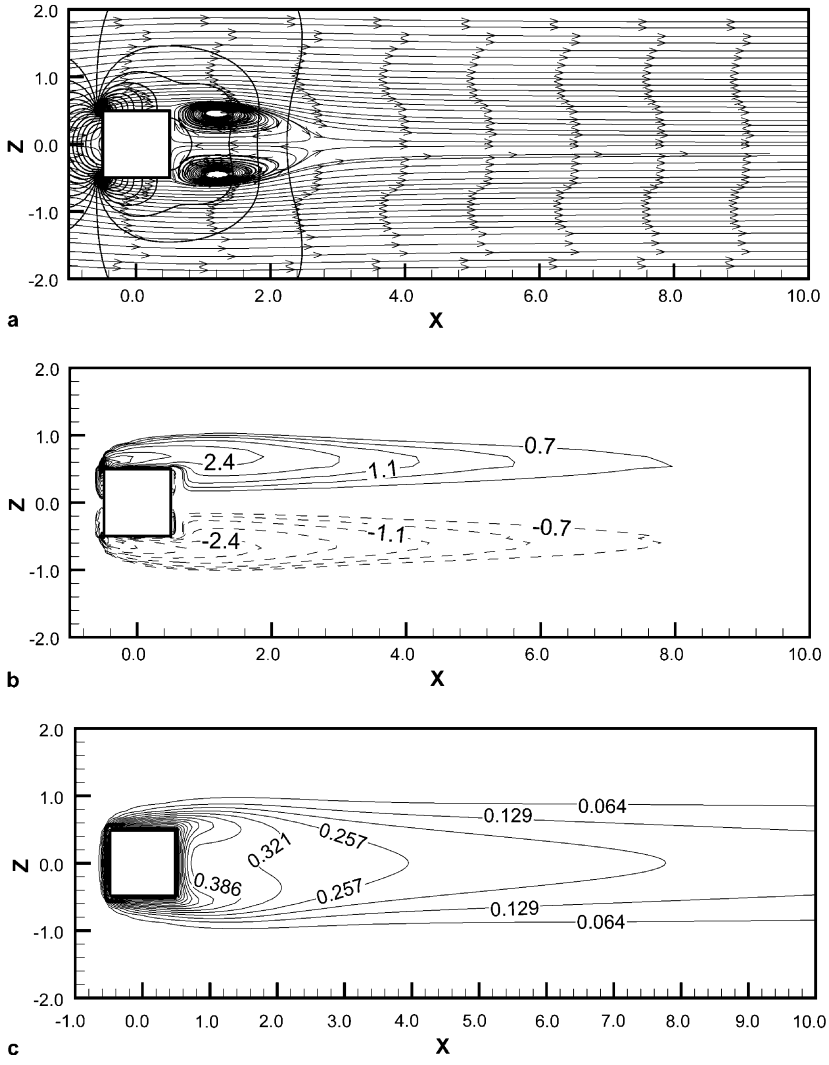

Fig. 2. (a) Streamlines (and pressure contours), (b) y-component (primary) vorticity, ω_y and (c) temperature contours on x–z plane at $Re = 200$.

front face of the cube experiences the high velocity flow, the temperature gradient on the front face is the highest among all the faces. On the other hand, the rear face of the cube shows the lowest heat transfer since it is adjacent to the recirculatory low velocity fluid region. Similar to the flow field, the temperature field also shows symmetric distribution about the wake centerline. The temperature gradient in the wake gradually decreases with the increase in the streamwise distance and the wake attains the free stream temperature. The uniformity of temperature in the far-wake is caused by the entrainment of the outer flow into the wake. As Reynolds number increases, the heat transfer from each side of the cube increases in the steady symmetric regime because of the increasing magnitude of forced convection. The size of the twin bubbles and their circulation strength increases with increasing Reynolds number and causes higher heat transfer from the rear face of the cube.

The distribution of Nusselt number on all the faces of the cube is depicted in Fig. 3 for $Re = 200$. The top figure in the first column shows the variation of Nusselt number on the front face of the cube. The heat transfer gradually increases towards the edges of the face. The reason for such a behaviour is due to the fact that the velocity near the center of the cube becomes low before hitting the face, while the flow turning along the front face, continues to accelerate and increases heat transfer. On the other hand, the heat transfer distribution on the rear face shows opposite trend as that of front face. The heat transfer near the edges is lower than the central region of the rear face. The flow behaviour near the rear face is similar to the impingement cooling where high velocity flow impinges on the surface and leaves the surface tangentially as shown in Fig. 2(a). The recirculating flow in the central region of the symmetric bubbles gives a flow similar to a jet impinging on a wall giving higher Nusselt number. All the side walls reveal identical spatial distribution of Nusselt number and confirms the symmetry of the wake. The heat transfer at the front or leading edges of these sides is found to be maximum and is minimum towards the trailing edges.

3.2. Steady asymmetric flow

The flow and thermal field is found to become asymmetric at $Re = 218$. Fig. 4 reveals the pressure contours on two orthogonal mid planes at $Re = 250$. It has been shown in Saha (2004) that the flow distribution on x–z plane is symmetric while it is asymmetric on the other orthogonal plane (x–y). The pressure distribution depicted in Fig. 4 also reiterates the same phenomenon by giving symmetric distribution on one plane while asymmetric on the other. This means that the symmetric flow at $Re = 216$ loses its symmetry only about the mid x–z plane retaining its symmetry about the mid x–y plane. The losing of symmetry about one of the orthogonal planes while maintaining symmetry about the other is also termed as *planar symmetry*. The pressure field in the region in front of the cube on both the planes are

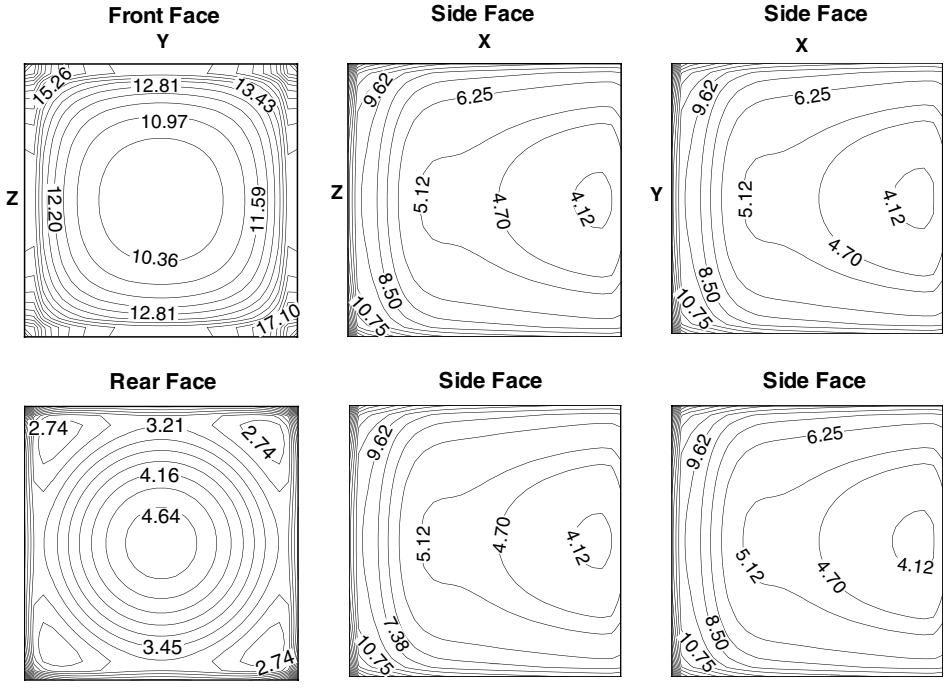

Fig. 3. Nusselt number contours at $Re = 200$. First column: Top figure corresponds to front face and bottom figure corresponds to rear face; Second and Third columns: side faces.

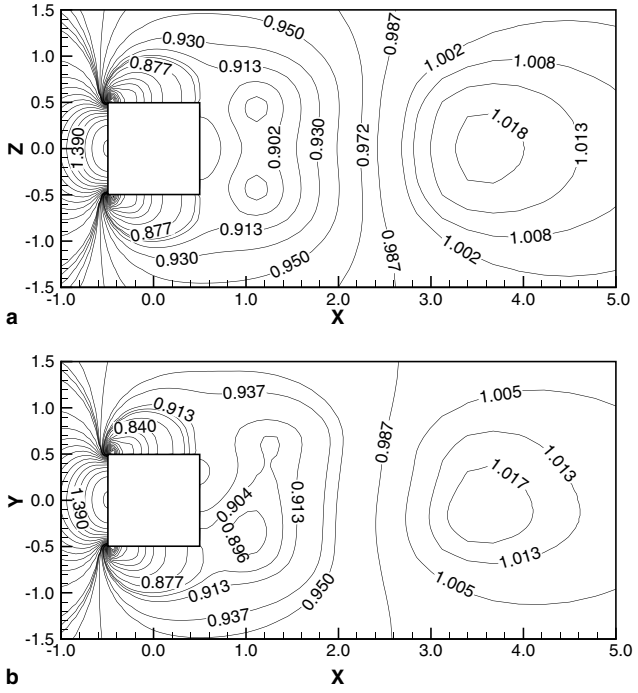

Fig. 4. Pressure contours at $Re = 250$ on (a) x–z and (b) x–y plane.

identical and starts deviating after the half width downstream from the leading edge. The corresponding temperature contours at $Re = 250$ on two different planes are presented in Fig. 5. Similar to the flow field, the temperature field also shows symmetry on one plane and asymmetry on the other and thus showing the evidence of planar symmetry even in the thermal field. The temperature distribution on the two orthogonal planes in the near wake ($x < 4.0$) shows little variation even though the strong effect of asymmetry is observed in the flow field. However, the far-wake shows almost identical temperature field on both the orthogonal planes showing no sign of asymmetry.

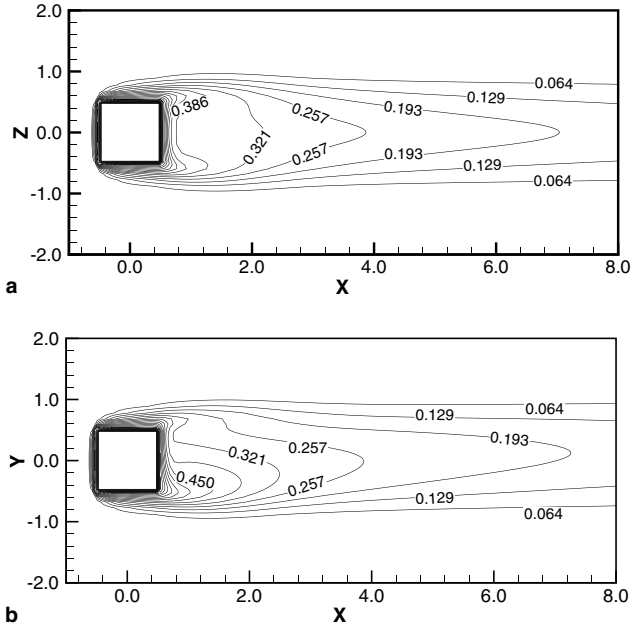

Fig. 5. Temperature contours at $Re = 250$ on (a) x–z and (b) x–y plane.

The spatial variation of Nusselt number on the various faces of the cube at $Re = 250$ has been demonstrated in Fig. 6. The distribution of Nusselt number at the front face is similar to that at $Re = 200$. However, the rear face shows asymmetric variation caused by the asymmetry of the flow and temperature fields. Since the approach flow is symmetric, the front face exhibits a symmetric distribution irrespective of the Reynolds number and transitions of the flow. The Nusselt number variation at the rear face is symmetric about the mid y-axis but asymmetric about mid z-axis. The asymmetry is also quite evident from Nusselt number distribution on the two opposite side faces. Since the flow and temperature fields show asymmetry about x–z plane, the side faces (parallel to x–z plane) reveal asymmetry in the heat transfer distribution. However, the Nusselt number variation on the other pair of opposite faces are exactly identical, showing the symmetric nature of thermal field about x–y plane. Compared to the distribution of Nusselt number at $Re = 200$ where one patch of high heat transfer on the side faces is observed, the variation at $Re = 250$ shows two such patches. The new additional patch is due to the small recirculatory region near all the side faces (not shown here).

3.3. Unsteady flow

The flow at $Re = 270$ undergoes a Hopf bifurcation and shows a time dependent behaviour while it shows a steady flow at $Re = 265$. Therefore, the critical Reynolds number for temporal transition is believed to lie between Reynolds numbers of 265 and 270. The unsteady flow has been computed for a small range of Reynolds number (270–400). Since the flow at $Re = 290$ is periodic with a dominant frequency, most of the unsteady dynamics are discussed using the results at this Reynolds number.

The temporal variation of drag and side force coefficients are presented in Fig. 7. The periodic nature of the flow is quite obvious from the sinusoidal nature of the drag and side force coefficients. The inset of the figure shows phase relationship among the drag coefficient, non-zero component of the side force coefficients and the Nusselt number. It is quite interesting to note that the two force coefficients have equal frequency and are in anti-phase. This means that the maxima in the side force corresponds to the minima in the drag coefficient. Unlike cube wake the flow past a square cylinder which is a two-dimensional counterpart of cube shows a frequency of drag coefficient that is twice that of lift coef-

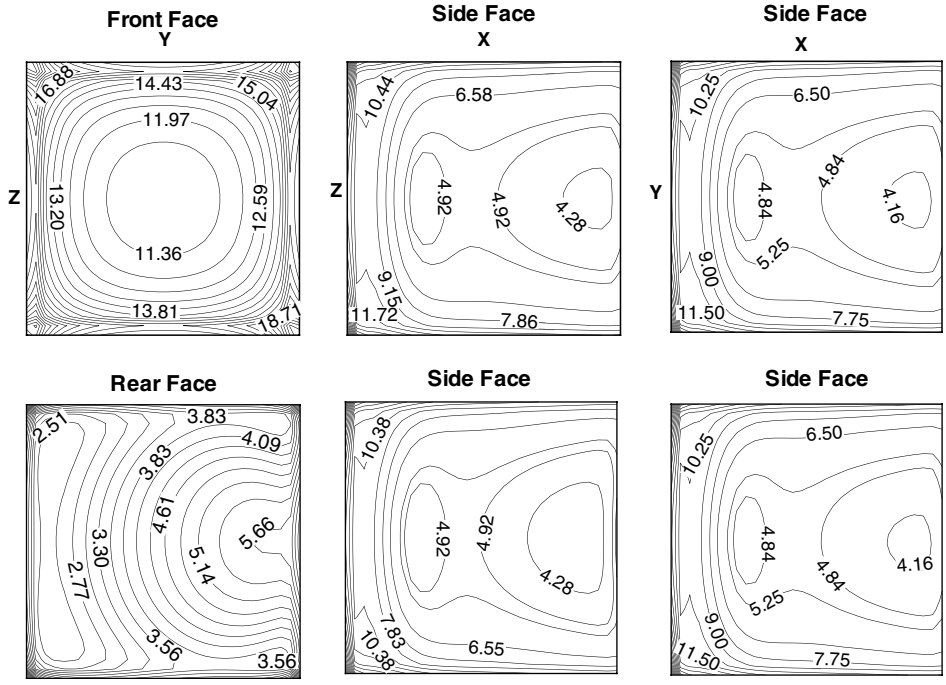

Fig. 6. Nusselt number contours at $Re = 250$. First column: Top figure corresponds to front face and bottom figure corresponds to rear face; Second and Third columns: side faces.

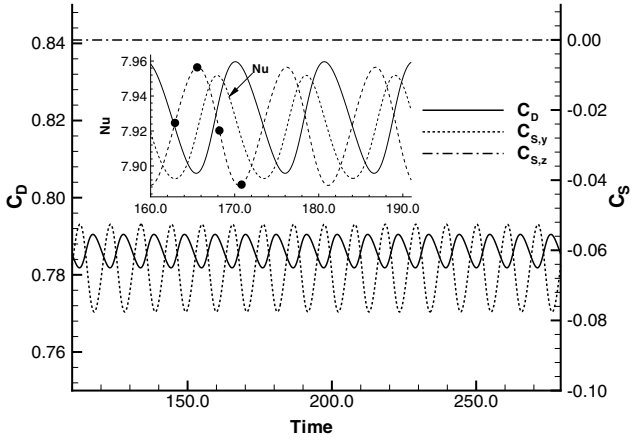

Fig. 7. Temporal variation of the drag, side force coefficients and Nusselt number of 290.

ficient. This is because of the two-sided nature of vortex shedding for the square cylinder wake. The time-averaged values of drag and y-component of side force coefficients are 0.786 and −0.065 and the respective rms values of fluctuations are 0.0030 and 0.0088 respectively. The time-mean and rms values of Nusselt number are found to be 7.92 and 0.0217 respectively. Since the flow is axisymmetric about the mid x–y plane, the z component side force is zero. The corresponding non-dimensional frequency of shedding of vortices, also called Strouhal number is 0.094. The phase relationship of the Nusselt number with the two force coefficients reveals that it is the average value of the two force coefficients.

The streamlines plots in Fig. 18 of Saha (2004) shows the distinct unsteadiness on one of the orthogonal planes while the flow remains steady symmetric on the other plane at $Re = 290$. From the streamlines (not shown here), it is seen that only the upper vortex detaches from the cube while the bottom vortex remains attached but alters its shape in response to the formation, topological changes and the subsequent shedding of the upper vortex. The growth and subsequent shedding of the upper vortex results in a one-sided vortex shedding. The one-sided vortex shedding of cube wake is responsible for the equal frequencies for the both drag and side force coefficients as seen in Fig. 7.

Fig. 8 depicts the unsteady variation of thermal field at the four different phases marked by filled circles in Fig. 7 (inset). Since only the upper vortex sheds downstream, the isotherms in the upper part of the wake changes while the isotherms in the lower part of the near-wake remains almost constant over the period. The temperature gradient in the lower region is smaller compared to the upper region near the rear face. This is due to the low velocity associated with the larger vortex adjacent to the bottom region of the rear face. The unsteady traveling wave of the thermal field of the wake is quite distinct from the streamwise convection of the valley in the temperature contours. Close examination of the streamlines (Fig. 18 in Saha, 2004) and the isotherms in Fig. 8 proves that the temperature contours are not fully correlated with the in-plane velocity field.

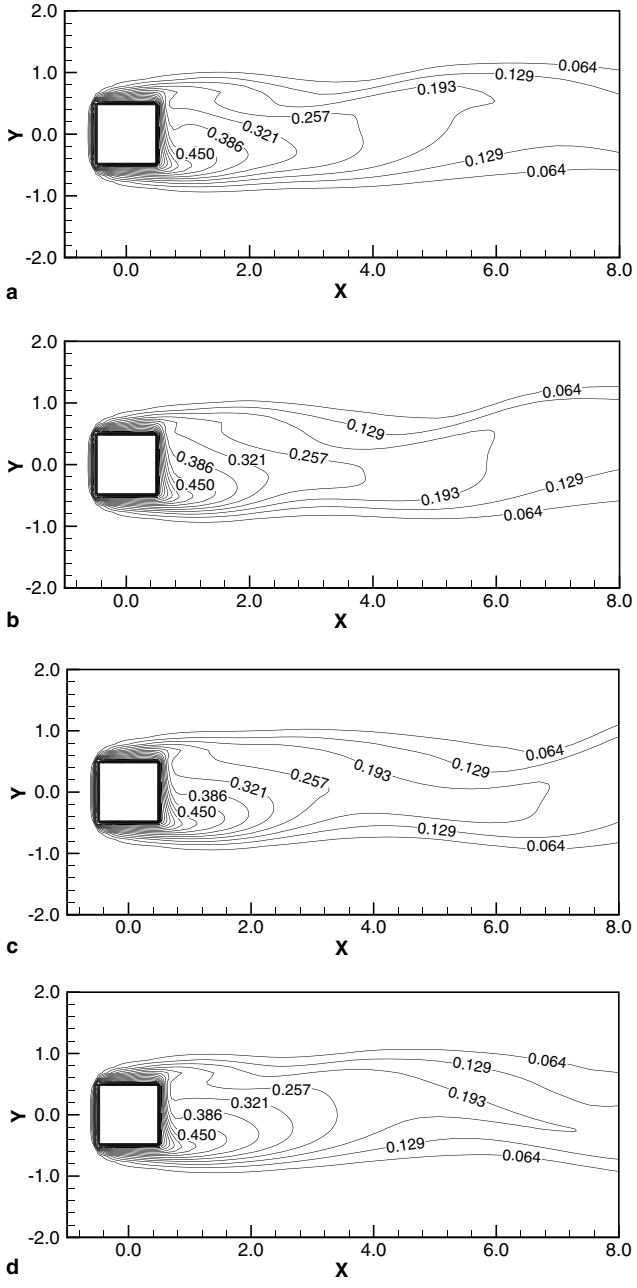

Fig. 8. Temperature contours on x–y plane at $Re = 290$: (a) $t = T/4$, (b) $t = 2T/4$, (c) $t = 3T/4$ and (d) $t = T$.

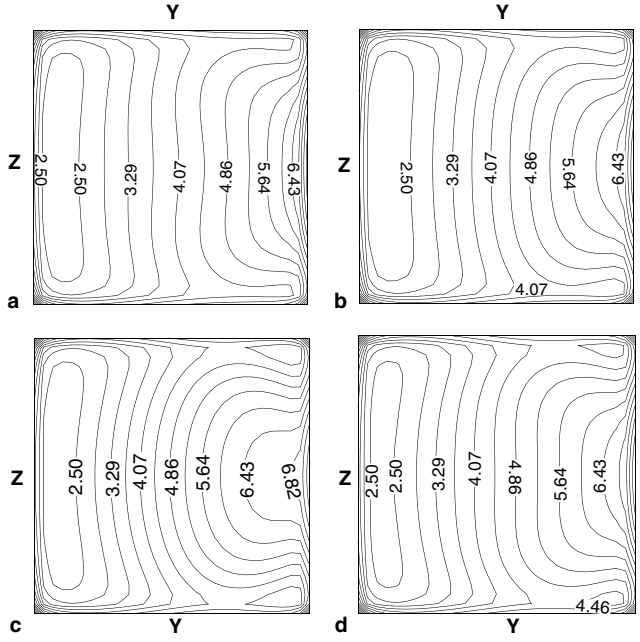

Fig. 9. Temporal variation of Nusselt number contours on the rear face at $Re = 290$: (a) $t = T/4$, (b) $t = 3T/4$, (c) $t = 3T/4$ and (d) $t = T$.

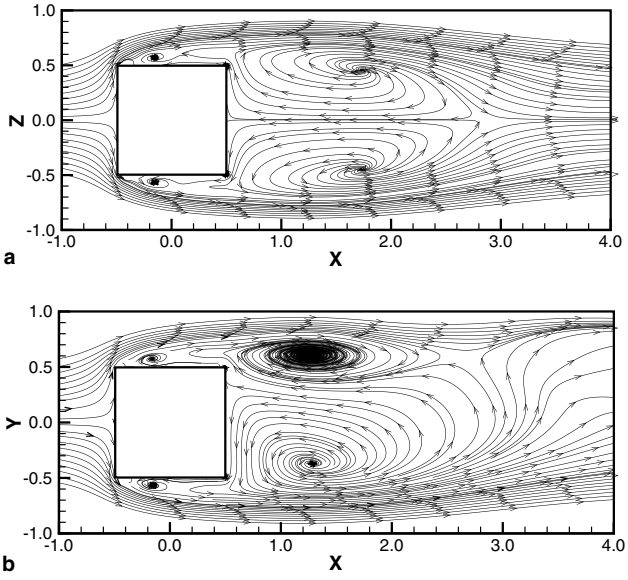

Fig. 10. Instantaneous streamlines at $Re = 325$ on (a) x–z and (b) x–y plane.

The contours of the instantaneous Nusselt number on the rear face of the cube at the four equally spaced phases are shown in Fig. 9. As the thermal field does not vary significantly over a period as seen in Fig. 8, the Nusselt number distribution reveals little variation over the period in relation to the formation of the upper vortex and its subsequent shedding.

With the increase in Reynolds number to 325, the wake becomes wider in one transverse direction while it shrinks in the other transverse direction. This particular fact is clear from the wake shown in Fig. 10. The planar symmetry of both the instantaneous velocity and thermal field is maintained and is clearly visible from symmetric distribution of velocity and temperature distribution on x–z plane and asymmetric distribution on x–y plane in Figs. 10 and 11. The temperature gradient on all the faces increases and results in higher value of Nusselt number (Fig. 12). The different pattern with non-identical values of Nusselt number (second column in Fig. 12) reveals distinct loss of symmetry at $Re = 325$.

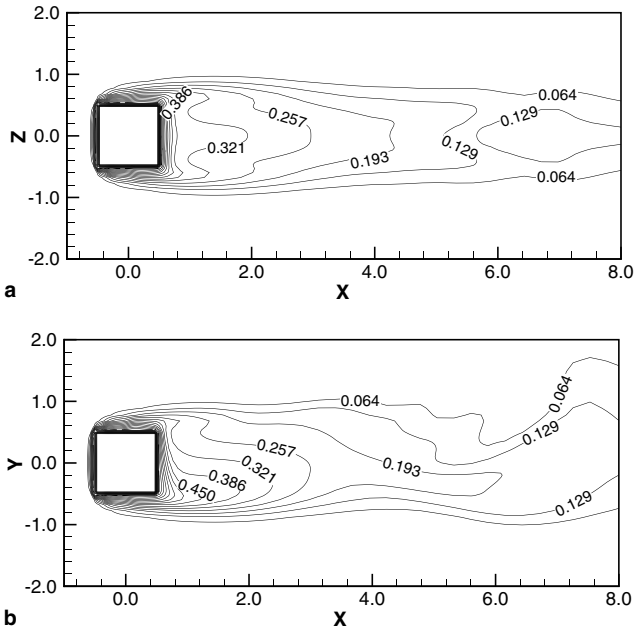

Fig. 11. Instantaneous temperature contours at $Re = 325$ on (a) x–z and (b) x–y plane.

On the other hand, the identical distribution of Nusselt number on the other two opposite side faces (third column in Fig. 12) proves the planar symmetry of the wake. The variation of the heat transfer on the two opposite side faces with asymmetric flow distribution shows different pattern than those at $Re = 250$ in Fig. 6. At $Re = 325$, the lower Nusselt number zones gets elongated and move towards the front (left) edges of the face. The symmetric variation of Nusselt number at the other two sides (x–y side) shows the similar trend of shifting their low heat transfer zones towards the front edges of the face. On the other hand, the rear face Nusselt number distribution shows significant difference as the isotherms becomes almost straight from curved ones at $Re = 250$ (see Fig. 6).

When the Reynolds number is increased to 400, the deviation from the planar symmetry is observed. At $Re = 400$, the symmetric flow and temperature distribution on x–z plane seen at $Re = 325$ is lost and have shown in Figs. 13 and 14. The comparison of the instantaneous flow structures near the cube reveals the generation of additional vortices and thus giving the multiple frequencies in the traces of drag and side force coefficients. The presence of these vortices makes the temperature distribution wavy very close to the wall. The temperature contours at $Re = 400$ shows more uneven variation with higher gradient near the wall. Fig. 15 shows temporal variation of drag force coefficients at two Reynolds numbers namely, 325 and 400. One interesting observation is that the drag coefficient is more for $Re = 400$ compared to that at $Re = 325$. This is just the opposite to the situation for Reynolds number range of $50 \leqslant Re \leqslant 325$ where it shows a decreasing trend. FFTs of the drag coefficient signal have also been shown in Fig. 15 (inset). Both at $Re = 325$ and 400, clear evidence of multiple frequencies is visible with more number of

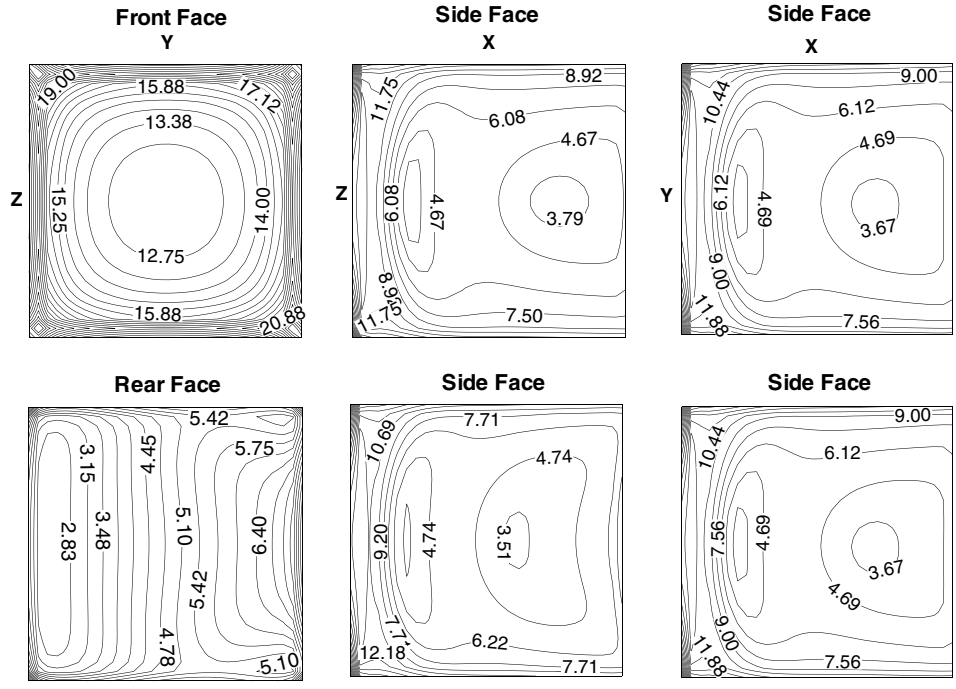

Fig. 12. Time-averaged Nusselt number contours at $Re = 325$. First column: Top figure corresponds to front face and bottom figure corresponds to rear face; Second and Third columns: side faces.

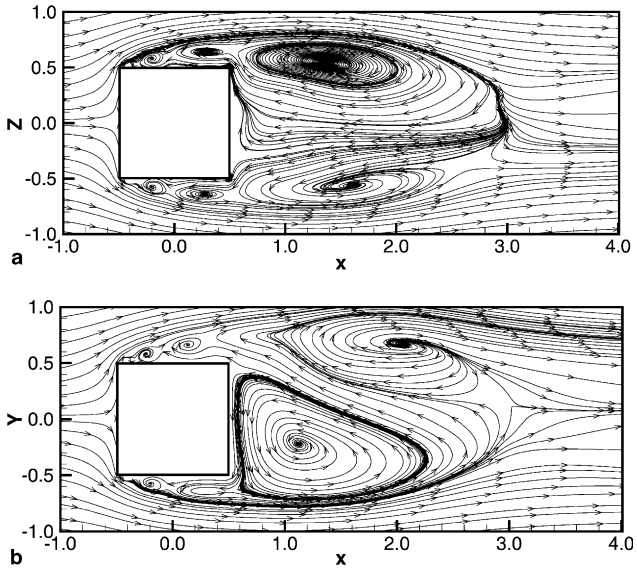

Fig. 13. Instantaneous streamlines at $Re = 400$ on (a) x–z and (b) x–y plane.

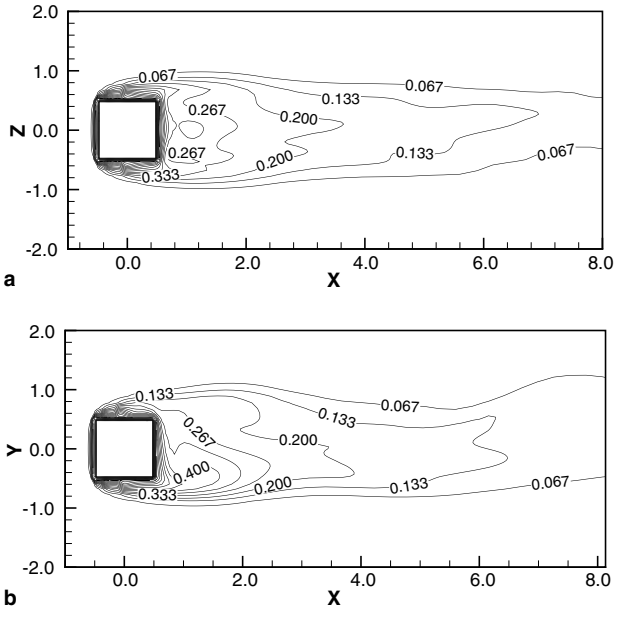

Fig. 14. Instantaneous temperature contours at $Re = 400$ on (a) x–z and (b) x–y plane.

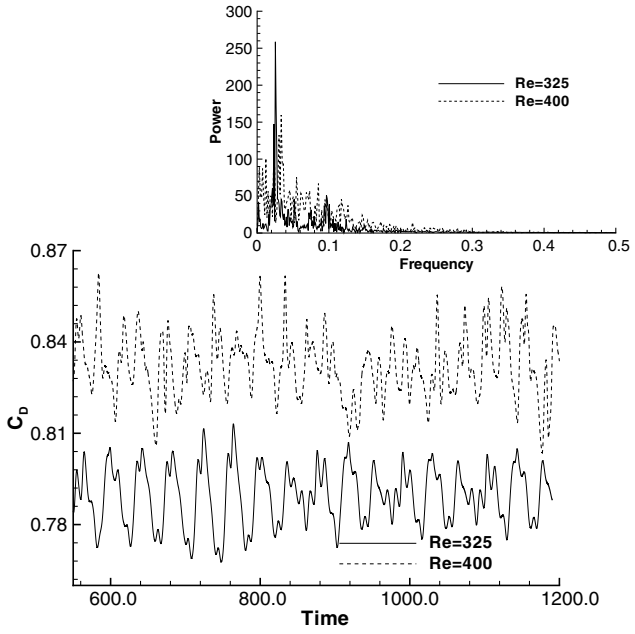

Fig. 15. Temporal variation of the drag force coefficient at Reynolds numbers of 325 and 400; Inset: corresponding FFTs.

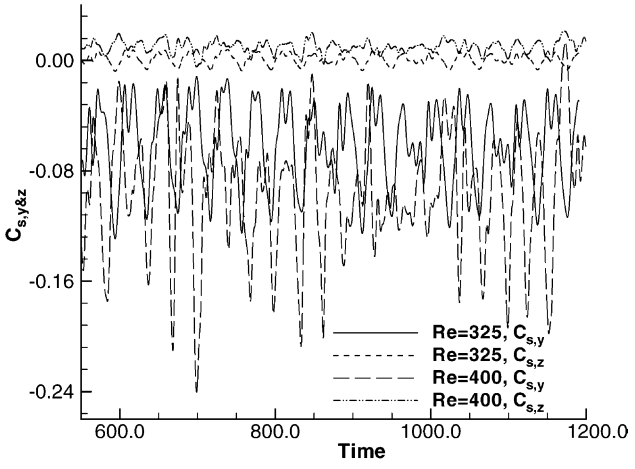

Fig. 16. Temporal variation of the side force coefficients at Reynolds numbers of 325 and 400.

frequencies at $Re = 400$. The temporal variation of two components of side force coefficients has also been depicted in Fig. 16. Close examination of the flow structures and the temporal variation of side force coefficients shown in Fig. 16 reveals that unlike at $Re = 290$ where the symmetric flow on x–z plane is almost steady (see Fig. 7), it is unsteady at $Re = 325$. It has been mentioned earlier that the planar symmetry breaks down at $Re = 400$ and this fact is quite obvious from the fluctuating non-zero side force coefficient ($C_{S,z}$). Similar observation of planar symmetry loss for a sphere wake is reported by Mittal (1999), Sakamoto and Haniu (1990) and Tomboulides and Orszag (2000). Mittal (1999) reports a comparable Reynolds number while it is higher for other two studies. With the increase in Reynolds number, the higher amplitude fluctuation of the other component of side force coefficient ($C_{S,y}$) suggests the increase in nonlinear interactions among the various scales (size of vortices) in the flow.

The dependency of Reynolds number on drag coefficient and overall (space and time-averaged for unsteady

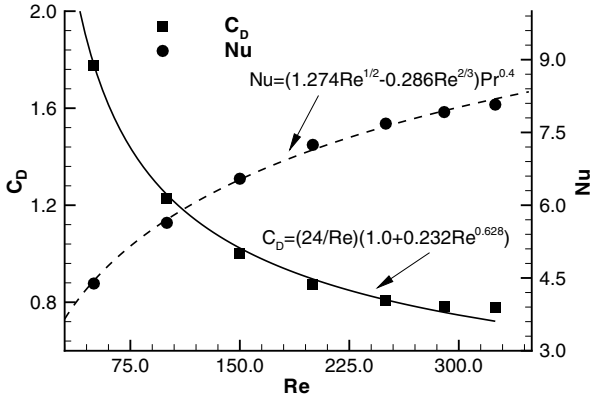

Fig. 17. Variation of drag forces and Nusselt number at various Reynolds numbers.

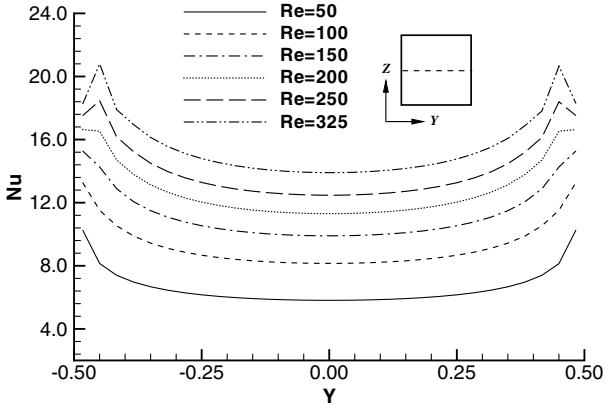

Fig. 18. Nusselt number variation at front face of the cube at various Reynolds numbers.

flow) heat transfer from cube surface is shown in Fig. 17. The drag coefficient is found to decrease while heat transfer increases with increasing Reynolds number. The minimum pressure within the recirculating bubble or vortex depends on the length of the recirculation length. The recirculation length is defined as the streamwise distance from the centre of the cube where the streamwise velocity changes its sign or where the shear layers rejoin. The increase in recirculation length decreases the base suction pressure. Since the drag coefficient is inversely related to the recirculation length, an increase in recirculation length corresponds to a decrease in drag coefficient and vice-versa. The initial strong dependency on the Reynolds number fades away with increasing Reynolds number and becomes almost independent of Reynolds numbers for $Re > 200$. The best-fit curve (solid line) through the points in Fig. 17 can be given by an expression $C_D = (24/Re)(1 + a \times Re^b)$ with $a = 0.232$ and $b = 0.628$. Similar expression of drag coefficient data ($a = 0.15$ and $b = 0.687$) for the sphere wake is also reported in Clift et al. (1978). Similarly, the curve-fit (dotted line) expression for Nusselt number values is given by $Nu = (1.274Re^{1/2} - 0.286Re^{2/3})Pr^{0.4}$. The flow past a sphere also show an increase in heat transfer with the increase in Reynolds number. Whitaker (1972) reported a best-fit curve for Nusselt number that is given by $Nu = 2 + (0.4Re^{1/2} + 0.06Re^{2/3})Pr^{0.4}$. At $Re = 325$, the maximum discrepancy between the data points and the curve-fit data for the drag coefficient and Nusselt number are 7.5% and 1.5% respectively. It is expected that the transition from a steady flow to an unsteady one brings about a sudden jump in the heat transfer because of the shedding of the vortices that carry hot fluid from the near wake to the far wake. Interestingly, no such behaviour is observed in the *Nu–Re* curve. Close examination of both the curves shows that at the low *Re* regime, the rate of decrease in drag coefficient is quite rapid while the increase in heat transfer is rather slow and this implies stronger dependency of drag coefficient on Reynolds number than the Nusselt number.

The line plot of Nusselt number (time-averaged values for unsteady flow) at the front face for various Reynolds number is presented in Fig. 18. It is worth to mention that the Nusselt number is averaged along the *z*-direction. Since the heat transfer at the front face is orthogonally symmetric irrespective of the various transitions, the *y*-direction averaged values also show similar variation of *Nu* in *z*-direction. As expected, the heat transfer shows a symmetric distribution because of the uniform incoming flow. The consistent increase in heat transfer is also quite distinct with the increase in Reynolds number because of increased convection with increasing Reynolds number. Fig. 19 shows the variations of Nusselt number at the rear face along both *y*- as well as *z*-directions. Similar to the front face, for the *y*-direction variation, the *Nu* is averaged along *z*-direction and vice-versa. The variation along *y*-direction in Fig. 19(a) shows that the thermal field remains symmetric up to $Re = 200$ but becomes asymmetric at $Re = 250$. The Nusselt number value near the bottom edge ($y \sim -0.5$) is almost constant at all Reynolds number while it increases towards the top edge in the asymmetric flow regime (both steady and unsteady). However, the planar symmetry of the wake gives a symmetric variation of heat transfer in *z*-direction (Fig. 19(b)). The continuous increase of heat transfer with increasing Reynolds number is also clear from both the figures. For the intermediate Reynolds number range, $150 \leqslant Re \leqslant 250$, the Nusselt number distribution shows a bulge at the center showing higher heat transfer at the center of the rear face.

3.4. Comparison with other bluff body wake

3.4.1. Square cylinder wake

It is to be noted that the square cylinder is a two-dimensional bluff body while the cube is a three-dimensional one. Both square cylinder and cube have identical

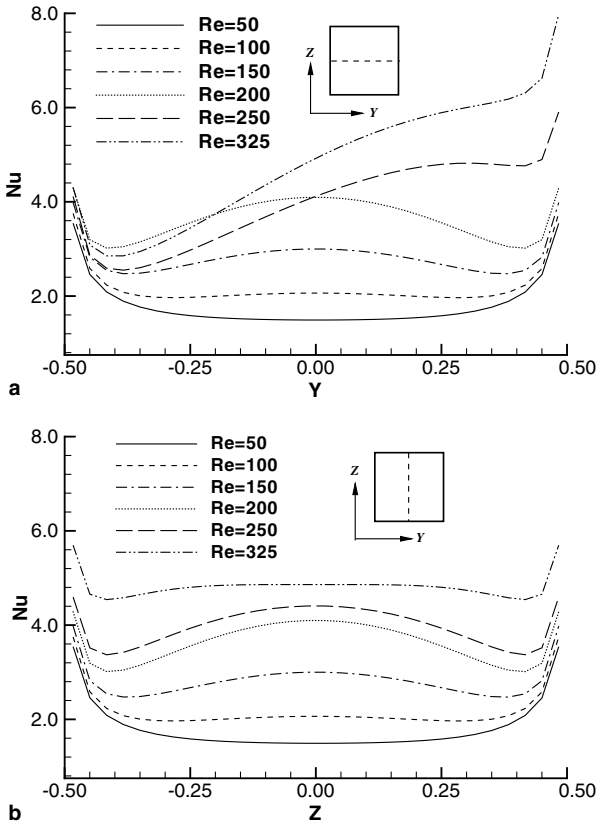

Fig. 19. Nusselt number variation at rear face of the cube at various Reynolds numbers.

separation mechanism (i.e. separation from the leading face edges). The flow characteristics past a square cylinder is well understood and documented in the literature. The two-dimensional steady wake behind a square cylinder undergoes a Hopf bifurcation at $Re \sim 50$ and becomes unsteady but remains two-dimensional. In contrast, the three-dimensional orthogonal-symmetric steady cube wake becomes steady asymmetric at $Re = 216$. The second transition for a square cylinder wake occurs at $Re = 175$ and is a spatial one in which two-dimensional flow becomes three-dimensional (Robichaux et al., 1999; Saha et al., 2003). But the cube wake undergoes a temporal transition (Hopf bifurcation) at $Re = 270$ but maintains its planar symmetry. For a square cylinder, the wake becomes dominated by multiple frequencies after $Re \sim 200$ while for a cube wake the corresponding Reynolds number is about 325.

Heat transfer from a square cylinder at low Reynolds number ($5 \leqslant Re \leqslant 160$), at which the flow remains two-dimensional, have been well documented in Sharma and Eswaran (2004). They reported correlations for average Nusselt number as a function of Reynolds number for both constant wall temperature and constant heat flux and are $Nu = 0.359\sqrt{Re} + 0.442$ and $Nu = 0.386\sqrt{Re} +$ 0.54 respectively. For $Re = 50$, they found the Nusselt number to be 2.98 while it is 4.39 for a cube (see Table 2). Similarly, the Nusselt numbers for square cylinder and cube wakes at $Re = 100$ are 4.03 and 5.64 respectively. The numerical investigation of heat transfer past a square cylinder by Kelkar and Patankar (1992) shows the Nusselt number at $Re = 100$ to be 3.25. It has been quite clear from the present study and the results presented by Sharma and Eswaran (2004) that the heat transfer from a cube is about 47% and 40% (with respect to square cylinder) higher than that of a square cylinder at $Re = 50$ and 100 respectively. The probable reason may be the three-dimensionality of the cube wake irrespective of Reynolds number.

3.4.2. Sphere wake

The transition phenomena of a sphere wake have been the subject of extensive research in the past. The transition sequence and shedding mechanism of a cube wake is found to be similar to that of a sphere wake. The separation mechanism and the integral parameters such as Strouhal number, side force and drag coefficients and Nusselt number are different from those of sphere wake although the macroscopic flow past a cube resembles to the flow past a sphere. The separation points are fixed for the sharp-edged cube at the front leading edges, but for a sphere, the separation points vary with Reynolds number and the other factors such as turbulence in the incoming flow. The sphere wake undergoes a transition to a steady asymmetric wake from a steady axisymmetric wake at a Reynolds number that lies in the range of 210–220 (Johnson and Patel, 1999; Bagchi et al., 2001; Tomboulides and Orszag, 2000). The present study of a cube wake shows the critical Reynolds number to fall in the range of 216–218.

The flow past a sphere undergoes a second transition, a Hopf bifurcation in the Reynolds number range of 270–285 at which the flow becomes unsteady (Bagchi et al., 2001; Johnson and Patel, 1999; Tomboulides and Orszag, 2000). The associated shedding frequency of unsteadiness at $Re = 300$ reported by the different researchers (Bagchi et al., 2001; Johnson and Patel, 1999; Tomboulides and Orszag, 2000) is in the range 0.134–0.137. The critical Reynolds number of unsteadiness in the present study for a cube wake has been found to be between 265 and 270. The corresponding Strouhal frequency at $Re = 300$ for the present study is 0.095, which is less than the sphere wake. With an increase in Reynolds number, the instantaneous cube wake shows a loss of planar symmetry i.e., the loss of symmetry on both orthogonal planes. Sphere wake also reveals similar planar symmetry loss (Mittal, 1999; Sakamoto and Haniu, 1990; Tomboulides and Orszag, 2000). The Reynolds number for the cube flow in the present study is found to be 400 while it is in the range of 350–375 for a sphere wake (Mittal, 1999). The corresponding values

Table 2
Comparison of integral parameters of cube and sphere

Re	Cube (Present study)		Sphere (Bagchi et al., 2001)		% Difference w.r.t sphere	
	$\overline{C}_D$	$\overline{Nu}$	$\overline{C}_D$	$\overline{Nu}$	$\overline{C}_D$	$\overline{Nu}$
50	1.78	4.39	1.57	5.43	13.38	19.15
100	1.23	5.64	1.09	6.91	12.84	18.38
200	0.87	7.24	0.77	9.09	12.99	20.35
250	0.81	7.68	0.70	9.94	15.71	22.74
325	0.78	8.07	0.64	11.26	21.88	28.33

in Sakamoto and Haniu, 1990 and Tomboulides and Orszag (2000) are 420 and 500 respectively.

Table 2 presents the comparison of the drag coefficient and Nusselt number of the present study and those of sphere wake reported in Bagchi et al. (2001) at various Reynolds numbers. For both cube and sphere, the drag coefficient decreases with the increasing Reynolds number. As the bubble grows in size the recirculation length increases and this in turn decreases the BSP. Consequently the drag force decreases with Reynolds number. The drag force is always higher for a cube than a sphere due to the higher bluffness associated with the cube. The Nusselt number also varies in a similar increasing trend as that of sphere wake. The drag coefficient for a cube wake is about 13–22% lower compared to the sphere wake. The heat transfer from a cube also shows a 19–29% lower values than the sphere for Reynolds number range of 50–325.

The above discussion reveals an important finding of the transition sequence of both the cube and sphere wakes. For both geometries, at around $Re \sim 215$–220, the three-dimensional axisymmetric steady flow becomes three-dimensional non-axisymmetric steady flow. At a relatively higher Reynolds number, $265 \leqslant Re \leqslant 285$, both wakes suffer a second transition which is a Hopf bifurcation and the flow shows unsteady behaviour with a three-dimensional non-axisymmetric wake.

4. Conclusion

Three-dimensional numerical study of flow past a cube in the Reynolds number range of 50–400 has been reported. The flow remains steady and symmetric up to a Reynolds number of 216. The flow becomes asymmetric about mid x–z plane at $Re = 218$ but maintains the symmetry about mid x–y plane. At $Re = 270$, the flow undergoes a Hopf bifurcation, and becomes unsteady but maintains planar symmetry. In the steady regime, the drag coefficient decreases with the increase in Reynolds number. On the other hand the drag force is found increase in the unsteady regime. Similar to the flow field, thermal field also shows the evidence of different transitions. The heat transfer from cube surfaces increases with the increase in Reynolds number. However, the switching from a steady to an unsteady flow does not show any jump in the heat transfer. The flow structures and the transition sequence of a cube wake are found to be identical to that of the sphere wake. At high Reynolds number ($Re > 325$), the flow starts losing its planar symmetry with increasing number of frequencies as the Reynolds number increases.

References

Achenbach, E., 1974. Vortex shedding from spheres. J. Fluid Mech. 62, 209–221.

Bagchi, P., Ha, M.Y., Balachandar, S., 2001. Direct numerical simulation of flow and heat transfer from a sphere in a uniform cross-flow. J. Fluids Eng., Trans. ASME 123, 347–358.

Constantinescu, G., Squires, K., 2004. Numerical investigation of flow over a sphere in the subcritical and supercritical regimes. Phys. Fluids 16, 1449–1466.

Clift, R., Grace, J.R., Weber, M.E., 1978. Bubbles, Drops and Particles. Academic Press, New York.

Hoffman, G., Benocci, C., 1994. Numerical simulation of spatially-developing planer jets. AGARD CP-551, 26.1–26.6.

Igarashi, T., 1985. Heat transfer from a square prism to an air stream. Int. J. Heat Mass Transfer 28, 175–181.

Johnson, T.A., Patel, V.C., 1999. Flow past a sphere up to a Reynolds number of 300. J. Fluid Mech. 378, 19–70.

Kelkar, K.M., Patankar, S.V., 1992. Numerical Prediction of vortex shedding behind a square cylinder. Int. J. Numer. Meth. Fluids 14, 327–341.

Kim, H.J., Durbin, P.A., 1988. Observations of the frequencies in a sphere wake and of drag increase by acoustic excitation. Phys. Fluids 31, 3260–3265.

Lyn, D.A., Einav, S., Rodi, W., Park, J.-H., 1995. A laser-Doppler velocimetry study of ensemble-averaged characteristics of turbulent near wake of a square cylinder. J. Fluid Mech. 304, 285–319.

Magarvey, R.H., Bishop, R.L., 1961. Transition ranges for three-dimensional wakes. Can. J. Phys. 39, 1418–1422.

Maxworthy, T., 1969. Experiments on the flow around a sphere at high Reynolds numbers. J. Appl. Mech. Trans. ASME E36, 598–607.

Mittal, R., 1999. Planar symmetry in the unsteady wake of a sphere. AIAA J. 37, 388–391.

Nakamura, I., 1976. Steady wake behind a sphere. Phys. Fluids 19, 5–8.

Natarajan, R., Acrivos, A., 1993. The instability of the steady flow past spheres and disks. J. Fluid Mech. 254, 323–344.

Orlanski, I., 1976. A simple boundary condition for unbounded flows. J. Comput. Phys. 21, 251–269.

Ranz, W.E., Marshall, W.R., 1952. Evaporation from drops. Chem. Eng. Prog. 48, 141–146.

Raul, R., Bernard, P.S., 1991. A numerical investigation of the turbulent flow field generated by a stationary cube. J. Fluids Eng., Trans. ASME 113, 216–222.

Raul, R., Bernard, P.S., Buckley Jr., F.T., 1990. An application of the vorticity-vector potential method to laminar cube flow. Int. J. Numer. Meth. Fluids 10, 875–888.

Renksizbulut, M., Yuen, M.C., 1983. Numerical study of droplet evaporation in a high-temperature stream. J. Heat Transfer, Trans. ASME 105, 389–397.

Robichaux, J., Balachandar, S., Vanka, S.P., 1999. Three-dimensional Floquet instability of the wake of square cylinder. Phys. Fluids 11, 560–578.

Saha, A.K., 2004. Three-dimensional numerical simulation of the transition of flow past a cube. Phys. Fluids 16, 1630–1646.

Saha, A.K., Muralidhar, K., Biswas, G., 2000. Transition and chaos in two-dimensional flow past a square cylinder. ASCE J. Eng. Mech. 126, 523–532.

Saha, A.K., Biswas, G., Muralidhar, K., 2003. Three-dimensional study of flow past a square cylinder at low Reynolds numbers. Int J. Heat Fluid Flow 24, 54–66.

Sakamoto, H., Haniu, H., 1990. A study on vortex shedding from spheres in a uniform flow. J. Fluids Eng., Trans. ASME 112, 386–392.

Sayegh, N.N., Gauvin, W.H., 1999. Numerical analysis of variable property heat transfer to a single sphere in high temperature surroundings. AIChE J. 25, 522–534.

Sharma, A., Eswaran, V., 2004. Heat and fluid flow across a square cylinder in the two-dimensional laminar flow regime. Numer. Heat Transfer Part A 45, 247–269.

Thomson, M.C., Leweke, T., Provansal, M., 2001. Kinematics and dynamics of sphere wake transition. J. Fluids Struct. 15, 575–585.

Tomboulides, A.G., Orszag, S.A., 2000. Numerical investigation of transitional and weak turbulent flow past a sphere. J. Fluid Mech. 416, 45–73.

Whitaker, S., 1972. Forced convection heat transfer correlations for flow in pipes, past flat plates, single spheres, and for flow in packed beds and tube bundles. AIChE J. 18, 361–371.